2014 IEEE International Conference on Robotics & Automation (ICRA)
Hong Kong Convention and Exhibition Center
May 31 - June 7, 2014. Hong Kong, China

Development and CPG-based Control of a Biomimetic Robotic Fish with Advanced Underwater Mobility

Yonghui Hu[1], Shuai Zhang[1], Jianhong Liang[2] and Tianmiao Wang[2]

Abstract— **This paper presents a biomimetic robotic fish that swims using thunniform kinematics for advanced underwater mobility. Propulsion and maneuvering of the robotic fish are achieved with a lunate caudal fin that undergoes combined translational and rotational motion. A parallel four-bar propulsive mechanism attached to the rear of the rigid torpedo-shaped body is used to deliver motor rotation to the caudal fin. Oscillatory control signals for the tail joints are generated with a CPG controller composed of two unidirectionally coupled Hopf oscillators. Coupling terms that allow direct specification of phase relation between oscillators are formulated. The maximum speed of the robotic fish can reach 2.0 m/s and excellent maneuverability has been exhibited. The outstanding swimming performances present exciting possibilities for real-world deployment of the robotic fish.**

I. INTRODUCTION

The process of evolution has produced highly effective biological mechanisms for aquatic locomotion. Fishes, as the ultimate examples of superior swimmers, have evolved an astonishing level of swimming capabilities, with some species able to cruise great distances at significant speed, while other species excel at dynamic stability in turbulent waters and low-speed maneuvers in tight spaces [1]. Recent years have witnessed a significant progress in the development of biomimetic underwater vehicles that propel and maneuver themselves utilizing fish-like movements [2]–[9]. The driving motivation for such research efforts is to achieve enhanced swimming performance in speed, efficiency, acceleration, agility and stealth over conventional propeller-driven underwater vehicles.

Despite extensive research efforts over the past two decades, most robotic fishes have remained merely laboratory curiosities. Reports on real-world applications of robotic fishes are very scarce, although it was anticipated that they would become highly functional platforms applicable for a wide range of underwater missions. The current situation is partly due to the increasingly demanding mission requirements, but more important is the fact that their swimming performances are far inferior to traditional unmanned underwater vehicles (UUV), not to mention their natural counterparts. According to the literature reports, the maximum speed attained by robotic fish is 1.36m/s [3], while the operational speed of UUV range from 0.5 to 5 m/s. Fish-like swimming has been proved more economical than screw propulsion in terms of hydrodynamic efficiency by a number of theoretical and experimental studies, but the reciprocating movements of fins require more complicated drive trains than the rotational motion of propellers, leading to lower overall efficiency. Further, the flexible body of robotic fish makes it difficult to install payload and to resist water pressure in deep diving. An obvious advantage that robotic fishes have exhibited lies in maneuverability, thanks to the use of multiple fins and flexible bodies. Fishes have undoubtedly provided an ideal solution to underwater locomotion, but their engineered replicas are still at an early stage of development. Knowledge from diverse disciplines, such as fish physiology, bio-hydrodynamics, artificial muscle technology and neuroscience-based control, should be integrated in order to bridge the gap between nature and engineering [10].

Today's UUV missions require a variety of capabilities: high speed, excellent maneuverability, long range and endurance, silent operation, great payload capacity, *et al*. Some of these requirements are mutually exclusive, which precludes the possibility of creating a versatile underwater platform suitable for a multitude of missions. The objective of current study is to develop a robotic fish for real-world exploration, probe and survey missions. Advanced underwater mobility, especially high cruising speed that is the most important requirement of such missions, is realized with specific design and control solutions. The robotic fish emulates thunniform propulsion optimized for high speed swimming with an oscillating caudal fin driven by a parallel four-bar mechanism. A rigid torpedo-shaped pressure hull, rather than flexible fish-shaped body, is adopted for the housing of power, electronics and payload. The locomotion controller is constructed based on a central pattern generator (CPG) model to generate robust, smooth and coordinated oscillatory control signals for the tail joints. Coupling terms that allow direct specification of phase shifts between translation and rotation of the caudal fin is formulated. The robotic fish achieves a maximum speed of 2.0 m/s during stable straight swimming and demonstrates excellent maneuverability. To the best of our knowledge, this is the fastest speed that robotic fishes have achieved.

II. MECHATRONIC DESIGN OF ROBOTIC FISH

A. Prototype Overview

Thunniform swimming is typical of some of the fastest marine vetebrates, such as scombrid fish, laminid sharks and cetaceans. The propulsive movements of thunniform swimmers are confined to the posterior one-third of the body. Thrust is generated primarily with a high aspect

[1]Yonghui Hu and Shuai Zhang are with School of Control and Computer Engineering, North China Electric Power University, Beijing 102206, P. R. China huyhui@gmail.com

[2]Jianhong Liang and Tianmiao Wang are with School of Mechanical Engineering and Automation, Beihang University, Beijing 100191, P. R. China

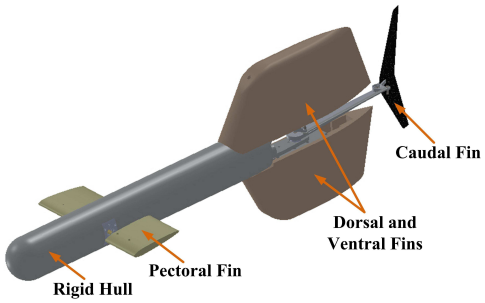

Fig. 1. Mechanical design of robotic fish.

TABLE I

TECHNICAL SPECIFICATIONS OF THE ROBOTIC FISH PROTOTYPE

Item	Characteristics
Dimension(L×W×H)	∼1180mm×330mm×400mm
Hull diameter	100mm
Displacement	∼11.6kg
Actuator	DC brush motors & servomotors
Operating mode	Radio control, 443MHz
Power supply	25.6V rechargeable LiFePO4 batteries
Maximum forward speed	2.0m/s
Minimum turning radius	0.58m

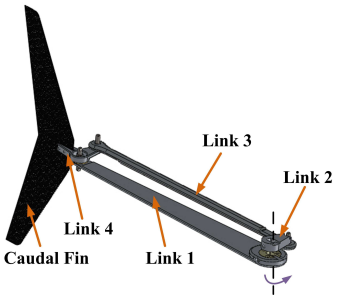

(a) Mechanical design.

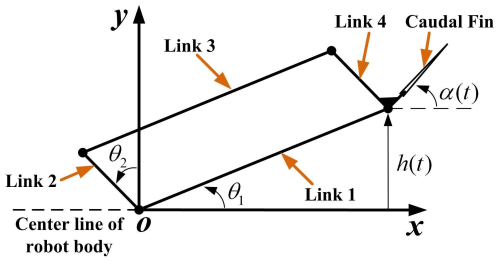

(b) Schematic illustration.

Fig. 2. Propulsive mechanism of robotic fish.

ratio, crescent-shaped caudal fin that undergoes a combined translational and rotational motion. The profile of attack angle is properly controlled throughout the stroke cycle to ensure high propulsive efficiency. These defining features of thunniform swimming have been implemented on the mission-scale, free-swimming robotic fish. Fig. 1 illustrates the mechanical configurations of the robotic fish.

The robotic fish employs a rigid torpedo-shaped body for housing of power, electronics and payload. Compared with the commonly used flexible fish-shaped body, such a design allows easy fabrication and excellent pressure resistance ability. The tail thruster, attached to the rear end of the hull, is composed of actuators, drive link assembly and a lunate caudal fin. Maxon RE40 DC motors are used as the actuators due to their simple controllability, high-speed operation and repeatability. The actuators are embedded in large dorsal and ventral fins, which are made of buoyancy material and help maintain stability. The drive link assembly is directly exposed to water, saving the energy to deform any flexible exostructures. The robotic fish is also equipped with a pair of pectoral fins, each actuated by a Hitec HS5645 servomotor. By adjusting the pitching angles of the pectoral fins, three-dimensional swimming as well as posture control can be realized. Table I lists the technical specifications of the robotic fish prototype.

B. Propulsive Mechanism

The propulsive mechanism that transmits motor torque to the caudal fin is based on a parallel four-bar mechanism. Fig. 2 shows the mechanical design and schematic illustration of the propulsive mechanism. It consists of four links connected by four revolute joints, forming a closed-loop mechanism. Link 1 and 2 are input links, driven by two motors that are installed coaxially at point O. The caudal fin is attached to link 4, which is L-shaped and rotates around the pivot at the corner. The oscillating motion of the caudal fin can be precisely controlled by the motors via the parallel four-bar mechanism.

The caudal fin of robotic fish, acting as a lift-generating hydrofoil, moves with a constant forward velocity and oscillates harmonically to trace a sinusoidal pathway that is symmetrical about the longitudinal axis of the body and in time. The harmonic oscillation of the caudal fin can be regarded as a combination of translational and rotational motion specified at the leading edge

$$h(t) = h_0 sin(2\pi ft) \tag{1}$$

$$\alpha(t) = \alpha_0 sin(2\pi ft + \psi) \tag{2}$$

where $h(t)$ is the transverse desplacement of the leading edge, $\alpha(t)$ is the angle between the leading edge and the longitudinal axis, h_0 is the translational amplitude, α_0 is the rotational amplitude, f is the tail beating frequency, and ψ is the phase difference between translation and rotation.

The oscillatory movement of the caudal fin is determined by the rotating angles of link 1 and 2. Given the kinematics of the caudal fin, the motor control law can be derived as

$$\theta_1(t) = arcsin(\frac{h_0}{l_1} sin(2\pi ft)) \tag{3}$$

$$\theta_2(t) = \alpha_0 sin(2\pi ft + \psi) \tag{4}$$

where $\theta_1(t)$ and $\theta_2(t)$ are rotating angles of the motors, l_1 is the length of link 1. The robotic fish can perform turning maneuvers by biasing the propulsive mechanism to one side of the body. Offset angles will be superposed on both degrees of freedom.

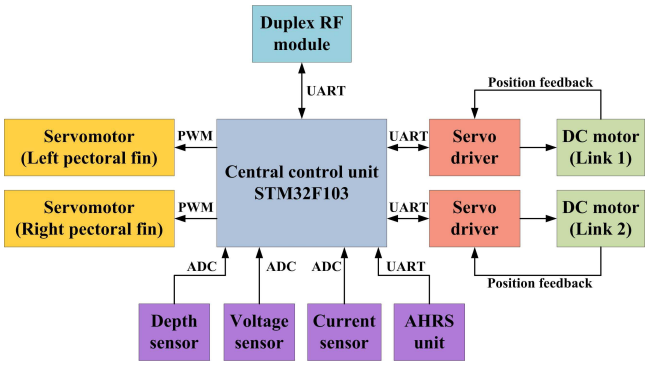

Fig. 3. Block diagram of the electrical system.

C. Electrical System

The on-board electrical system of the robotic fish provides power, actuation, sensing, control and communication functions. A high capacity rechargeable LiFePO4 battery pack allows power autonomy of three hours at cruising speed. The central control unit is a microcontroller STM32F103 that incorporates a high performance 32-bit RISC, ARM Cortex-M3 core running at 72 MHz from STMicroelectronics. The DC motors are driven and controlled by two servo drivers from UPTECH Robotics. The sensor suite includes depth sensor, voltage sensor, current sensor and an AHRS unit. High-level steering and speed inputs, as well as on-board sensor readings are delivered through a duplex RF module. Fig. 3 illustrates the block diagram of the electrical system.

III. CPG-based Locomotion Control

Locomotion control of the robotic fish can be achieved with online gait generation and tracking control. The motor control law specified by equation (3) and (4) can be used to calculate the target angles for the tail joints, which will then be sent to the servo drivers. The explicit relationship between tail kinematics and the control law allows easy adjustment of the swimming gait. However, online modification of the control parameters will cause discontinuous jump of joint angles, which might damage the actuator and the propulsive mechanism. Inspired by the neurobiological principle of locomotor rhythmogenesis, CPG-based locomotion controller have been designed and implemented on a variety of biomimetic robots [11]. CPGs are specialized neuronal circuits capable of producing coordinated patterns of rhythmic activity without any rhythmic inputs from sensory feedback or from higher control centers. The advantages of CPG-based control approach include stable rhythm generation, smooth gait transition, robustness to perturbation and easy integration of sensory feedback signals. In this paper, a CPG controller with explicit parameter controlling phase difference between oscillatory CPG units is built for locomotion control of the robotic fish.

In robotic applications, CPG is modeled as an assembly of neural oscillators that spike periodically through reciprocal inhibition. Among various mathematical models of neural oscillator, Hopf oscillator is widely used as the basic oscillatory unit of the CPG controller [12]–[14]. Hopf oscillator can generate self-sustained sinusoidal oscillation and has explicit parameters for setting frequency and amplitude. Its dynamic behavior is described by the following nonlinear differential equations

$$\begin{cases} \dot{u} = (\rho - r^2)u - \omega v \\ \dot{v} = (\rho - r^2)v + \omega u \end{cases} \tag{5}$$

where $r = \sqrt{u^2 + v^2}$, u and v are state variables in Cartesian space, $\rho > 0$ controls the amplitude of the oscillation, and ω specifies the intrinsic frequency of the oscillator (in rad s^{-1}). The Hopf oscillator has a harmonic limit cycle, and the steady state solution can be written as $u_\infty(t) = \sqrt{\rho}cos(\omega t + \phi_0)$ and $v_\infty(t) = \sqrt{\rho}sin(\omega t + \phi_0)$, where ϕ_0 is determined by the initial condition. The analytical solution of the oscillator facilitates parameter specification for a desired oscillation profile. Furthermore, the limit cycle is structurally stable, which means small perturbations will be forgotten and the trajectory will converge back to the limit cycle.

Each CPG unit is responsible for generating the oscillatory behavior of one tail joint. The state variable u of the oscillator is taken as the CPG output, which determines the target angular position of the joint. In order to achieve appropriate phasing between joints, the oscillators should be connected together. The desired locomotor pattern given by equation (3) and (4) can be realized with appropriate coupling scheme and parameter setting. Generally, the coupling term from one oscillator to another is implemented as an additive perturbation, which influences phase dynamics of the forced oscillator, leading to frequency synchronization and stable phase shifts between them. However, the oscillation amplitude of the forced oscillator will also be modified, which makes it hard to specify parameter for a desired oscillation amplitude. In order to eliminate this undesirable side effect, the perturbation signal p is required to act on the state variables of the forced oscillator in the following way [14]

$$\begin{cases} \dot{u} = (\rho - r^2)u - \omega v + \dfrac{\epsilon p v^2}{r} \\ \dot{v} = (\rho - r^2)v + \omega u - \dfrac{\epsilon p u v}{r} \end{cases} \tag{6}$$

where $\epsilon > 0$ denotes a constant coupling strength. By setting $u = rcos\phi$ and $v = rsin\phi$, equation (6) can be transformed into polar coordinates

$$\begin{cases} \dot{r} = (\rho - r^2)r \\ \dot{\phi} = \omega - \epsilon p sin\phi \end{cases} \tag{7}$$

It's obvious that the amplitude remains unperturbed and only the phase is affected, which means the perturbation acts only in the direction tangential to the limit cycle.

Following the tail structure of the robotic fish, a CPG network composed of two coupled Hopf oscillators, is constructed for generation of swimming gaits. For the sake of simplicity, only descending couplings are assumed, which follows that the rotational motion is perturbed by the translational motion. Fig. 4 shows the configuration of the CPG network. For the uni-directionally coupled network, desired phase relation between oscillators can be realized with a

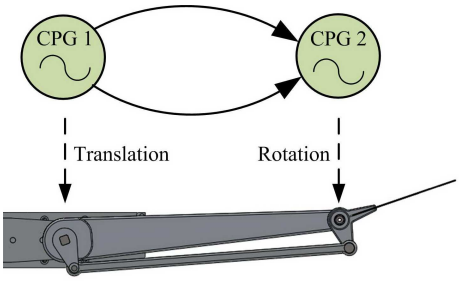

Fig. 4. Configuration of CPG network.

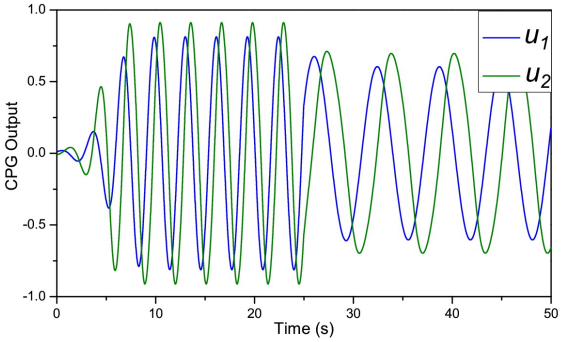

Fig. 5. CPG outputs during start and transition of commanded gaits. The initial states are set as $(u_1, v_1) = (0.01, -0.01)$ and $(u_2, v_2) = (-0.01, -0.01)$. Before $t = 25$, $\omega_1 = \omega_2 = 2.0$, $\rho_1 = 0.64$, $\rho_2 = 0.81$ and $\phi_d = \pi/3$. After $t = 25$, $\omega_1 = \omega_2 = 1.0$, $\rho_1 = 0.36$, $\rho_2 = 0.48$ and $\phi_d = \pi/2$. The constant $\epsilon = 0.5$.

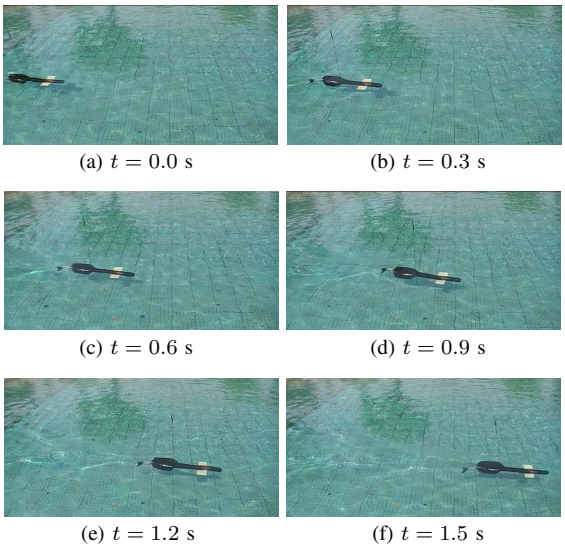

(a) $t = 0.0$ s (b) $t = 0.3$ s (c) $t = 0.6$ s (d) $t = 0.9$ s (e) $t = 1.2$ s (f) $t = 1.5$ s

Fig. 6. Snapshot sequence of straight swimming.

composite signal coming from the two state variables of the forcing oscillator, which are $\pi/2$ out of phase [14]. Each of the state variables produces a phase-attractive force on the phase point of the forced oscillator, resulting in a tendency for in-phase synchronization. By adjusting the relative strengths of components of the signal, a steady phase-locked state with arbitrary phase difference can be attained. However, tuning of the coupling strengths for a desired phase relation presents a challenging problem, which requires complex search, optimization or learning techniques. In the present study, an alternative formulation of the coupling model that allows direct specification of the phase relation is proposed. Instead of instantaneous coupling, the oscillators is assumed to interact via time-delayed coupling. Thus the forced oscillator can be modeled by

$$\begin{cases} \dot{u_2} = (\rho_2 - r_2^2)u_2 - \omega_2 v_2 + \dfrac{\epsilon u_1(t-\tau)v_2^2}{r_2} \\ \dot{v_2} = (\rho_2 - r_2^2)v_2 + \omega_2 u_2 - \dfrac{\epsilon u_1(t-\tau)u_2 v_2}{r_2} \end{cases} \tag{8}$$

where τ is the coupling delay. With this setting, the forced oscillator can be in-phase synchronized by the delayed state of the forcing one. Delay of the state variable corresponds to some phase shift in polar coordinates. By exploiting the circular symmetric property of the Hopf oscillator, one can derive the following relation

$$\begin{aligned} u_1(t-\tau) &= r_1 cos\phi_1(t-\tau) \\ &= r_1 cos(\phi_1 - \phi_d) \\ &= r_1(cos\phi_1 cos\phi_d + sin\phi_1 sin\phi_d) \\ &= u_1 cos\phi_d + v_1 sin\phi_d \end{aligned} \tag{9}$$

where ϕ_d is the phase shift caused by the delay. Substitution of equation (9) into (8) yields

$$\begin{cases} \dot{u_2} = (\rho_2 - r_2^2)u_2 - \omega_2 v_2 + \dfrac{\epsilon(u_1 cos\phi_d + v_1 sin\phi_d)v_2^2}{r_2} \\ \dot{v_2} = (\rho_2 - r_2^2)v_2 + \omega_2 u_2 - \dfrac{\epsilon(u_1 cos\phi_d + v_1 sin\phi_d)u_2 v_2}{r_2} \end{cases} \tag{10}$$

Therefore the desired phase difference can be attained by feeding weighted states u and v of one oscillator to the other, with sine and cosine functions of the phase difference as the coupling weights.

The rhythm-generating ability of the CPG network has been examined with numerical simulations. Fig. 5 shows the CPG outputs during start and transition of commanded gaits. The states of the CPG network starts from some random points other than the origin of the phase plane and asymptotically converge to stable limit cycles. Tuning of the CPG parameters enables the system to switch to new limit circles quickly and smoothly. The desired phase difference has been exactly exhibited by the two gaits, thereby validating the effectiveness of the proposed coupling scheme.

IV. Experimental Results

Experiments with the robotic fish are carried out in an outdoor swimming pool with still water of 1.2 m in depth. Swimming speed and maneuvering performances have been the focus of the experiments.

A. Testing of Swimming Speed

In speed tests, the robotic fish is required to swim along a straight line and the control parameters are fixed in each run. Measurements of average linear speed in steady state are obtained using video analysis method. Fig. 6 shows a snapshot sequence of straight swimming. Kinematic parameters that affect swimming speed include tail beating frequency,

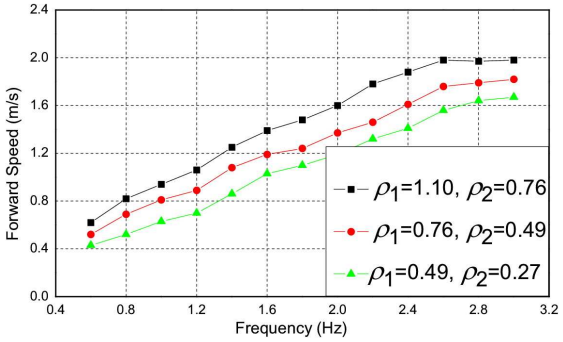

Fig. 7. Forward speed with different tail beating frequencies and amplitudes.

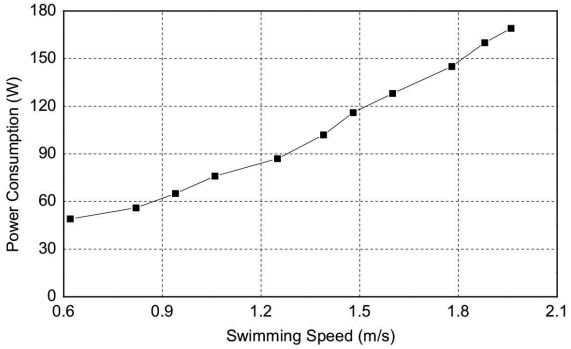

Fig. 8. Power consumption versus swimming speed.

amplitude and phase difference between translation and rotation. Several studies have revealed that maximum thrust can be obtained with phase difference of $\pi/2$ [16], therefore all tests have been conducted under this condition. Three groups of amplitude are tested, with frequency varied in each case. Fig. 7 shows the dependence of forward speed on tail beating frequency and amplitude. As illustrated, the forward speed increases almost linearly with the frequency, and large amplitude can also provide more thrust. At higher frequencies, the desired amplitudes can hardly be reached and the speed saturates due to the performance limits of the motors. At frequency of about 2.8 Hz, a maximum speed of 2.0 m/s is reached, which is approximately 1.7 BL/s (body length per second). A thorough literature review suggests that the robotic fish has outperformed all other robotic fish prototypes in terms of both absolute speed and length-specific speed.

The remarkable swimming speed is achieved at the expense of high power consumption. Due to the reciprocating motion of the motors and the complex hydrodynamic loads on the tail fin, the instantaneous power consumed by the tail thruster fluctuates drastically. To calculate the average power consumption, the following equation is employed

$$P = \frac{1}{T}\int_0^T U(t)I(t)dt \tag{11}$$

where $U(t)$, $I(t)$ and T are measured motor voltage, current and period, respectively. Fig. 8 shows the power consumption

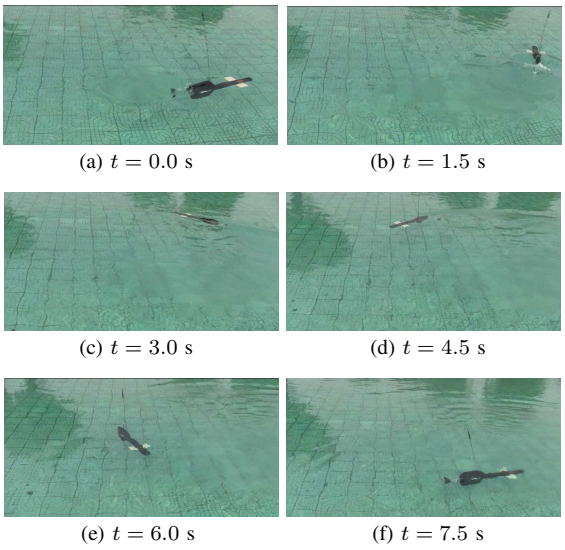

Fig. 9. Snapshot sequence of circular turning maneuvers.

versus swimming speed. Notice that the measured power is the total power consumed by the propulsion system. In order to reduce power consumption and increase propulsive efficiency of the robotic fish, proper selection of kinematic parameters, optimized design of the drive link assembly and vortex sensing and control techniques should be investigated.

B. Testing of Maneuvering Performances

Planar turning maneuvers of the robotic fish is tested by biasing the propulsive mechanism to one side of the robot. In order to achieve tail biasing, the state variable u of the CPG model is substituted by a new variable $u' = u - o$, where o is an offset angle. Fig. 9 shows a snapshot sequence of circular turning maneuvers. The performance of turning maneuvers can be evaluated in terms of turning radius and turning rate. In all tests, the same offset angle has been applied to the two tail joints. The dependence of turning performance on offset angle as well as tail beating frequency is illustrated in Fig. 10 and Fig. 11. For a constant frequency, the turning radius decreases while the turning rate increases with increasing offset angle. The increase of frequency results in larger turning rate, but the turning radius changes only slightly. It should be remarked that the robotic fish can turn with a very small turning radius when the tail flaps very slowly (for instance, below 0.3 Hz). Such an extreme maneuver can hardly be used in practice and is not considered in the experiments. A minimum turning radius of 0.92 BL and a maximum turning rate of 58 deg/s are achieved with offset angle of 50 deg and tail beating frequency of 2.8 Hz.

Thunniform swimmers, optimized for high-speed swimming, are not well-suited for turning maneuvers. Compared with robotic fish swimming with anguilliform or carangiform mode, the developed robotic fish turns with larger turning radius and cannot perform C-shaped sharp turning. However, the turning performances achieved by the robotic fish are outstanding among its kind. The VCUUV robotic fish, driven

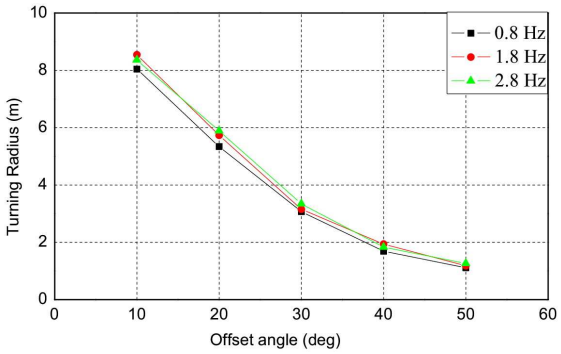

Fig. 10. Turning radius with different offset angles and tail beating frequencies.

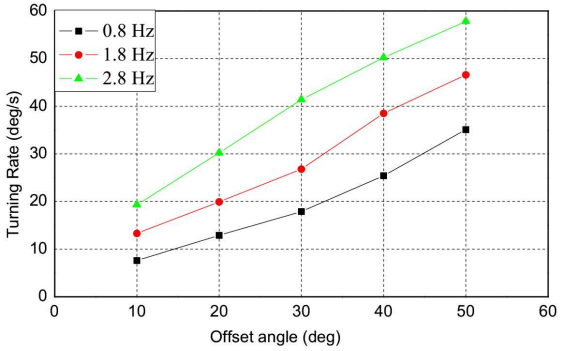

Fig. 11. Turning rate with different offset angles and tail beating frequencies.

by a four-joint caudal fin, achieves a minimum turning radius of 1 BL and a maximum turning rate of 75 deg/s [2]. The SPC-III robotic fish, a predecessor of the current robot, also achieves a minimum turning radius of 1 BL, but the maximum turning rate is only 35 deg/s [3]. Although the robotic fish is designed as a cruising-type underwater platform, the excellent maneuverability enables it to perform close inspection, rapid course adjustment and operation in cluttered environments.

V. Conclusions and Future Works

The emulation of fish swimming for UUV propulsion presents exciting possibilities for mobility improvements over traditional designs. The robotic fish presented in this paper, by adopting thunniform kinematics and mechanical design of high thrust-to-mass ratio, has been able to achieve significant speed and excellent maneuverability. The CPG controller allows generation of smooth, adaptive and coordinated oscillatory control signals for the tail joints. Experimental results have verified the effectiveness of proposed design and control approaches.

Future work will include dynamic modeling of the robot and experimental characterization of its propulsive efficiency. Design, sensing and control techniques for efficient swimming will be explored and investigated experimentally. A more sophisticated control system capable of mission planning and decision making will be developed for autonomous operation in real-world UUV missions.

Acknowledgements

This work was supported by the National Natural Science Foundation of China under Grant 61105108.

References

[1] M. Sfakiotakis, D. M. Lane, and J. Bruce C. Davies, Review of fish swimming modes for aquatic locomotion," *IEEE J. Oceanic Eng.*, vol. 24, no. 2, pp. 237-252, 1999.

[2] J. M. Anderson and P. A. Kerrebrack, "The vorticity control unmanned undersea vehiclełAn autonomous vehicle employing fish swimming propulsion and maneuvering," in *Proc. Int. Symp. UUST*, Durham, NH, Sep.1997, pp. 189-195.

[3] J. Liang, T. Wang, and L. Wen, "Development of a two-joint robotic fish for real-world exploration ," *J. Field Robot.*, vol. 28, no. 1, pp. 70-79, 2011.

[4] Z. Chen, S. Shatara, and X. Tan, "Modeling of biomimetic robotic fish propelled by an ionic polymerCmetal composite caudal fin," *IEEE/ASME Trans. Mechatronics*, vol. 15, no. 3, pp. 448-459, 2010.

[5] M. Aureli, V. Kopman, and M. Porfiri, "Free-locomotion of underwater vehicles actuated by ionic polymer metal composites," *IEEE/ASME Trans. Mechatronics*, vol. 15, no. 4, pp. 603-614, 2010.

[6] J. Tangorra, C. Phelan, C. Esposito, and G. Lauder, "Use of biorobotic models of highly deformable fins for studying the mechanics and control of fin forces in fishes," *Integr. Comp. Biol.*, vol. 51, no. 1, pp. 176-189, 2011.

[7] C. Zhou and K. H. Low, "Design and locomotion control of a biomimetic underwater vehicle with fin propulsion," *IEEE/ASME Trans. Mechatronics*, vol. 17, no. 1, pp. 25-35, 2012.

[8] K. W. Moored, T. H. Kemp, N. E. Houle, and H. Bart-Smith, "Analytical predictions, optimization, and design of a tensegrity-based artificial pectoral fin," *Int. J. Solids Struct.*, vol. 48, no. 22-23, pp. 3142-3159, 2011.

[9] O. M. Curet, N. A. Patankar, G. V. Lauder, and M. A MacIver, "Mechanical properties of a bio-inspired robotic knifefish with an undulatory propulsor," *Bioinsp. Biomim.*, vol. 6, pp. 026004, 2011.

[10] P. R. Bandyopadhyay, "Trends in biorobotic autonomous undersea vehicles," *IEEE J. Oceanic Eng.*, vol. 30, no. 1, pp. 109-139, 2005.

[11] A. J. Ijspeert, "Central pattern generators for locomotion control in animals and robots: A review," *Neural Netw.*, vol. 21, pp. 642-653, 2008.

[12] L. Righetti and A. J. Ijspeert, "Pattern generators with sensory feedback for the control of quadruped locomotion," *Proc. IEEE Int. Conf. Robotics and Automation*, May 2008, pp. 819-824.

[13] K. Seo, S. Chung, and J. E. Slotine, "CPG-based control of a turtle-like underwater vehicle," *Auton. Robot.*, vol. 28, no. 3, pp. 247-269, 2010.

[14] T. Wang, Y. Hu, and J. Liang, "Learning to swim: a dynamical systems approach to mimicking fish swimming with CPG," *Robotica*, vol. 31, no. 3, pp.361-369, 2013.

[15] A. Pikovsky, M. Rosenblum, and J. Kurths, *Synchronization: A universal concept in nonlinear sciences*. Cambridge University Press, Cambridge, 2001.

[16] Y. Park, U. Jeong, J. Lee, S. Kwon, H. Kim, and K. Cho, "Kinematic condition for maximizing the thrust of a robotic fish using a compliant caudal fin," *IEEE Trans. Robot.*, vol. 28, no. 6, pp. 1216-1227, 2012.